

Journal of Biomedical Optics

SPIEDigitalLibrary.org/jbo

Polarization speckle imaging as a potential technique for *in vivo* skin cancer detection

Lioudmila Tchvialeva
Gurbir Dhadwal
Harvey Lui
Sunil Kalia
Haishan Zeng
David I. McLean
Tim K. Lee

Polarization speckle imaging as a potential technique for *in vivo* skin cancer detection

Lioudmila Tchvialeva,^a Gurbir Dhadwal,^a Harvey Lui,^{a,b} Sunil Kalia,^a Haishan Zeng,^{a,b} David I. McLean,^a and Tim K. Lee^{a,b,c}

^aVancouver Coastal Health Research Institute and University of British Columbia, Department of Dermatology and Skin Science, Photomedicine Institute, Vancouver, V5Z 4E8, Canada

^bBC Cancer Agency, Departments of Cancer Control Research and Integrative Oncology, Vancouver, V5Z 1L3, Canada

^cSimon Fraser University, School of Computing Science, Burnaby, V5A 1S6, Canada

Abstract. Skin cancer is the most common cancer in the Western world. In order to accurately detect the disease, especially malignant melanoma—the most fatal form of skin cancer—at an early stage when the prognosis is excellent, there is an urgent need to develop noninvasive early detection methods. We believe that polarization speckle patterns, defined as a spatial distribution of depolarization ratio of traditional speckle patterns, can be an important tool for skin cancer detection. To demonstrate our technique, we conduct a large *in vivo* clinical study of 214 skin lesions, and show that statistical moments of the polarization speckle pattern could differentiate different types of skin lesions, including three common types of skin cancers, malignant melanoma, squamous cell carcinoma, basal cell carcinoma, and two benign lesions, melanocytic nevus and seborrheic keratoses. In particular, the fourth order moment achieves better or similar sensitivity and specificity than many well-known and accepted optical techniques used to differentiate melanoma and seborrheic keratosis. © The Authors. Published by SPIE under a Creative Commons Attribution 3.0 Unported License. Distribution or reproduction of this work in whole or in part requires full attribution of the original publication, including its DOI. [DOI: 10.1117/1.JBO.18.6.061211]

Keywords: polarization; depolarization ratio; automatic skin cancer detection; laser speckle; statistical moments.

Paper 12590SSP received Sep. 5, 2012; revised manuscript received Oct. 23, 2012; accepted for publication Oct. 24, 2012; published online Dec. 12, 2012.

1 Introduction

Due to recent advancements,¹ polarization has been utilized in a number of optical techniques such as fluorescence, Raman and reflectance spectroscopy, and proven to be effective for biomedical diagnosis. In this paper, we focus on skin polarimetry—applying a polarization speckle technique for detecting malignancy of skin lesions. Skin cancer is the most common cancer in the western world, and its incidence has been increasing steadily and rapidly in the last 40 years.^{2,3} Among the three common types of skin cancers (malignant melanoma, squamous cell carcinoma, and basal cell carcinoma), malignant melanoma is most fatal. The five-year survival rate for advanced cases is only 15%; however, melanoma is also almost 100% curable in an early stage.⁴ Furthermore, melanoma is sometimes difficult to diagnose because it often resembles benign skin lesions such as nevus and seborrheic keratosis. Currently, biopsy, an invasive medical procedure, is the gold standard for diagnosing skin cancer. Thus, developing polarization techniques for skin cancer detection may help diagnose the disease noninvasively at an early stage, when the prognosis is excellent.

Polarization has been widely used in dermatology. The technique can be generally divided into two schemes: polarization imaging, a manifestation of depolarization effect due scattering, and tissue characterization based on intrinsic polarimetry.

Dermoscopy⁵ is a well-known dermatological tool that can be implemented with polarization imaging methods. Based on the technique known as “polarization gating,”⁶ this common

tool can perform optical sectioning and reveal either surface or subsurface features of a skin lesion. The optical ability is explained by a two-layer polarization model where backscattered light from the surface and the superficial layer retains the linear polarization of the illumination, while the backscattered light from the deeper layer is depolarized. Directing an output polarizer to be parallel or perpendicular with respect to the input polarizer, an observer can select the depth of the backscattered signal. In particular, dermoscopists have developed a set of complex diagnostic rules for skin cancer according to the visual, subsurface dermoscopic features or patterns such as asymmetry, irregular borders and colors, irregular pigment networks, etc.⁷ Another polarized imaging technique augments polarization gating by computing the depolarization ratio $D = (I_{||} - I_{\perp}) / (I_{||} + I_{\perp})$ spatially, where $I_{||}$ and I_{\perp} denote the parallel and perpendicular backscattered polarized intensities, respectively, and form a two-dimensional (2-D) image.⁸ The advantage of the depolarization ratio image is that it preferentially captures the fraction of photons that travel only a few mean free paths,⁹ where one mean free path is approximately 100 μm for epidermis and dermis.¹⁰ Thus, depolarization ratio images encompass the epidermis and superficial dermal layers from where skin lesions often originate.¹¹ Jacques et al. suggested that the full margin of a skin lesion, that fails to be observed under a naked-eye examination, can be outlined using a depolarization ratio image.⁸ Although these two polarization imaging techniques assist physicians in diagnosing skin cancers, these techniques require qualitative assessment of the polarized images and do not fully exploit the intrinsic polarization properties of skin tissue. Hence, the full potential of polarization measurements is not realized.

Address all correspondence to: Tim K. Lee, BC Cancer Research Centre, Cancer Control Research Program, 675 West 10th Avenue, Vancouver, BC, Canada V5Z 1L3. Tel: +604-675-8053; Fax: 604-675-8180; E-mail: tlee@bccrc.ca

Skin components like collagen and keratin alter polarization via birefringence, optical activity and diattenuation.¹² These intrinsic changes of polarization can be evaluated quantitatively and used to classify tissue from different organs *in vitro*.¹³ Angelsky et al.¹⁴ successfully applied this approach to characterize thinly sliced tissue samples from heart, kidney, and spleen. However, the main drawback of the tissue polarimetry is the difficulty in measuring and analyzing the subtle polarization transformations distorted by random depolarization. Also collecting the necessary data for the quantitative analysis, which is based on one of two mathematical formulations: the Stokes-Mueller¹⁵ and Jones matrixes,¹⁴ is time-consuming. To apply either of the above two formulations, one needs to perform a set of measurements with the aid of polarizer-analyzer rotations. This time-consuming task represents a significant technical challenge to translate the technique into a real-time clinical application for skin cancer detection since body movements degrade the accuracy of intrinsic polarimetry methods.

In this paper, we demonstrate a new *in vivo* method that may become useful for skin lesion detection. The method combines the depolarization ratio D used in the polarization imaging with the quantitative analysis common in polarimetry. Unlike Jacques et al.'s depolarization ratio image,⁸ we computed depolarization ratios from the intensities of the backscattered speckle patterns, which are commonly modeled as two cross-polarized free-space speckle patterns $I_{||}$ and I_{\perp} .¹⁶ We captured these speckle patterns simultaneously with analyzers oriented parallel and perpendicular to the initial polarization, and generated a new 2-D pattern of the depolarization ratio. The resulting pattern, the polarization speckle pattern, is a stochastically distributed area field with

various polarization states. Examples of polarization speckle patterns are shown in Fig. 1. We believe that the distribution of the polarization speckle pattern captures vital information for skin cancer detection, and propose to analyze the polarization speckle pattern quantitatively using statistical moments. We hypothesized that using statistical moments of the polarization speckle pattern D would allow us to develop a fully automated diagnostic indicator for classifying different types of common skin lesions. To demonstrate the feasibility of our hypothesis, we conducted an *in vivo* clinical study, testing whether our method could statistically differentiate melanoma, squamous cell carcinoma, basal cell carcinoma, melanocytic nevus and seborrheic keratosis.

2 Materials and Methods

We conducted a clinical study of five types of malignant and benign skin lesions (malignant melanoma, squamous cell carcinoma, basal cell carcinoma, melanocytic nevus, and seborrheic keratosis), at the Skin Care Centre, Vancouver General Hospital. The diagnoses for the malignant lesions (malignant melanoma, squamous cell carcinoma, and basal cell carcinoma) were confirmed by biopsy. This study was approved by the UBC Clinical Research Ethics Board (study number H06-70281). Lesion measurements were acquired from patients attending a general dermatology clinic using a specially constructed laser speckle device.

The speckle device uses dual cameras to simultaneously capture two speckle patterns. (Fig. 2) Skin lesions were illuminated sequentially by two diode lasers, a blue laser ($\lambda = 407$ nm, 20 mW, BWB-405-20E, B&W Tek Inc., coherence length is

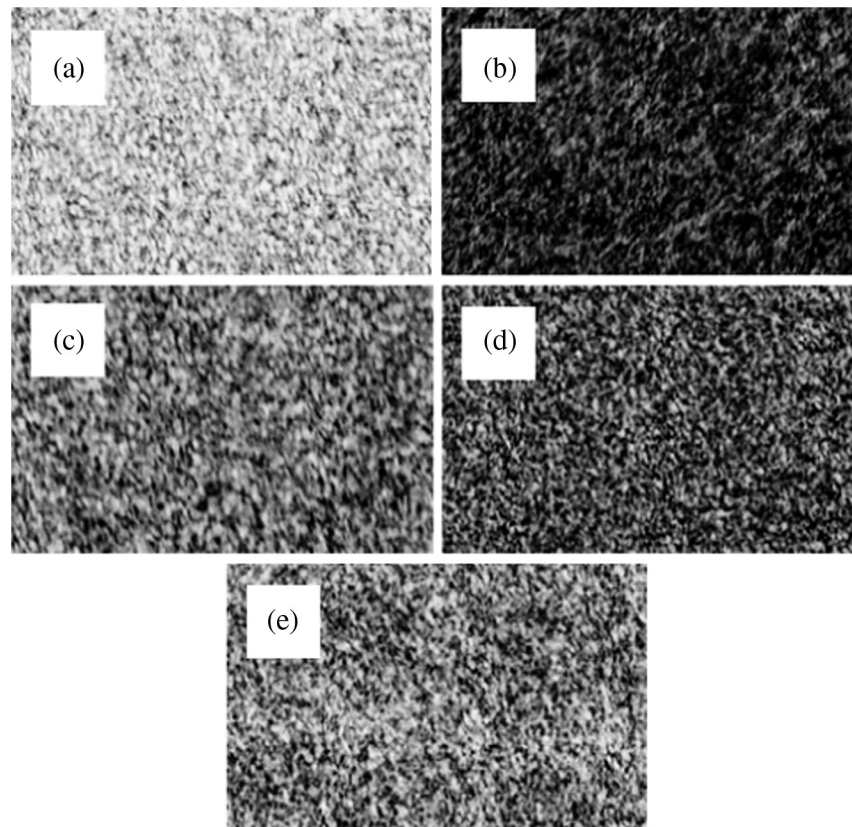


Fig. 1 Examples of polarization speckle patterns for (a) malignant melanoma, (b) squamous cell carcinoma, (c) basal cell carcinoma, (d) nevus, and (e) seborrheic keratosis using the blue laser (407 nm).

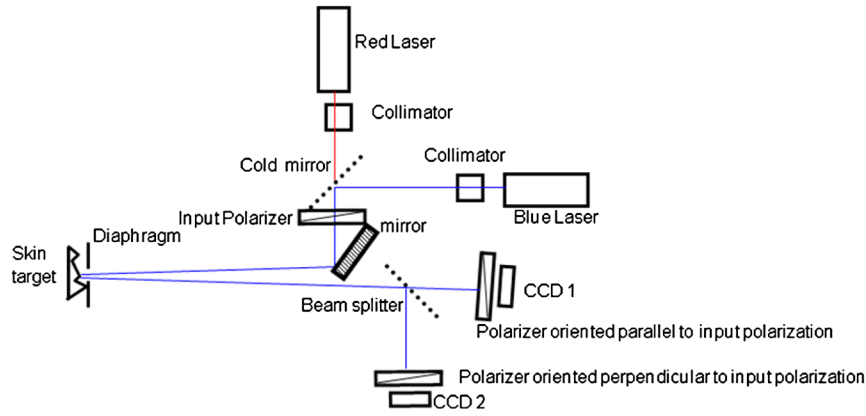


Fig. 2 The schematic of the laser speckle device.

about $200\ \mu\text{m}$ and a red fiber-coupled laser ($\lambda = 663\ \text{nm}$, 22 mW, 57PNL054/P4/SP, Melles Griot Inc., coherence length is about $300\ \mu\text{m}$). Using two lasers allowed us to study the effects of differences in absorption and depth of light penetration. Different tissues can be characterized by different combinations of absorption and scattering. According to Ref. 10, for example, normal skin has four times stronger absorption and scattering in the blue spectral region than in the red region. Penetration depth for the light which maintains its initial polarization was estimated based on Ref. 6 to be about 2.7 mean free paths (MFP). Consequently, the depth of light penetration for normal skin is about $50\ \mu\text{m}$ for the blue laser and about $200\ \mu\text{m}$ for the red laser. The average thickness of epidermis is about $100\ \mu\text{m}$ ¹⁷; therefore, the blue polarization speckle primarily relates to the epidermis layer while the red polarization speckle encodes information for the dermo-epidermal junction zone as well as the superficial dermis layer.

The angle of incidence was minimized to within 2 deg. from the normal direction of the skin surface. The backscattered signals were observed in the specular direction. A diaphragm limits the catchment area diameter to 3 mm. It enhanced signal-to-noise ratio¹⁸ by suppressing backscattered light from the surrounding normal skin. Scattered light was split into two beams by a pellicle beam splitter. The setup was designed in a such way that one camera captured 45% of *s*-polarized light while another one captured 35% of *p*-polarized light. Two beams generate two free-space speckle patterns captured by two identical charge coupled device (CCD) cameras (Matrix Vision GmbH, mvBlueFOX-M124G) without lenses. The patterns were recorded simultaneously by both cameras. One camera captured light parallel to the initial polarization (*s*-component regarding beamsplitter), and another one—perpendicular to the initial polarization (*p*-component regarding beamsplitter). The integration time was 5 ms to minimize signal distortion due to skin motion.

Signal processing included dark signal subtraction and a rigid registration between the parallel- and perpendicular-polarized speckle patterns. As the two cameras were placed at equal distances from the beam splitter, the two speckle images were in a general alignment. To further ensure pixel-by-pixel correspondence, we implemented a camera alignment procedure to generate the rotation, scaling and translation parameters for a rigid registration program, thereby producing two fully registered speckle patterns.

A polarization speckle pattern $D(x, y)$ was then calculated from the two registered parallel- and perpendicular-polarized speckle patterns using Eq. (1):

$$D(x, y) = \frac{I_{\parallel}(x, y) - I_{\perp}(x, y)}{I_{\parallel}(x, y) + I_{\perp}(x, y)}, \quad (1)$$

where $I_{\parallel}(x, y)$ and $I_{\perp}(x, y)$ were the pixel intensities of the corresponding parallel- and perpendicular-polarized speckle patterns. Two such $D(x, y)$ patterns of each lesion were calculated separately for the blue and red lasers.

The first to fourth order statistical moments of the polarization speckle pattern $D(x, y)$ were calculated based on the following equations:

$$M = \frac{1}{N} \sum_1^N |D(x, y)|, \quad (2)$$

$$\sigma = \frac{1}{N} \sum_1^N D(x, y)^2, \quad (3)$$

$$A = \frac{1}{\sigma^{3/2}} \left[\frac{1}{N} \sum_1^N D(x, y)^3 \right], \quad (4)$$

$$E = \frac{1}{\sigma^2} \left[\frac{1}{N} \sum_1^N D(x, y)^4 \right]. \quad (5)$$

We followed Angelsky et al.'s notation of naming these four moments as M , σ , A , and E .¹⁴ The variable N in Eqs. (2) to (5) denotes the total number of pixels in the polarization speckle pattern.

To perform statistical analyses on the moments of the polarization speckle pattern, we utilized the Kruskal-Wallis test with Dunn's multiple comparison posttest (Prism 5 for Windows, GraphPad Software, La Jolla, California). The α significance level was set to 0.05. The statistical software identified all significantly different pairs with three significance levels, $p < 0.05$, < 0.01 , and < 0.001 .

3 Results

We examined 214 skin lesions including the three major types of skin cancers, malignant melanoma (MM), squamous cell carcinomas (SCC), and basal cell carcinomas (BCC), and two benign conditions, melanocytic nevus (nevus), and seborrheic keratoses (SK) (Table 1).

Figure 1 shows examples of the polarization speckle patterns $D(x, y)$ captured and calculated for each lesions type using Eq. (1). The theoretical range of $D(x, y)$ is from 0 to 1 where $D(x, y) = 1$, the white polarization speckle, marks a linear polarized area, and $D(x, y) = 0$, the black speckle, denotes mostly fully depolarized light. The gray speckles in between relate to the partially depolarized light.

Figure 3 shows the box-and-whisker plots for the first to fourth order statistical moments of the polarization speckle patterns $D(x, y)$ calculated using Eqs. (2) to (5), for the blue and red lasers separately.

All moment distributions showed differences among the five lesion types for all four moment analyses ($p = 0.0001$ for all Kruskal-Wallis tests). The results of Dunn's multiple comparison tests are presented in Tables 2 and 3 for the blue and red lasers, respectively.

According to Table 2, the blue laser could be used to differentiate MM from other skin lesions except nevus. All four moments could be used for such a task. However, the fourth order statistical moment E seems to be the most efficient. On the other hand, the red laser was more suitable for SK identification (Table 3). Again, the fourth order moment E seems to work better than the other three moments.

4 Discussion

We believe the polarization speckle pattern $D(x, y)$, generated by Eq. (1), is a convenient tool for *in vivo* skin lesion differentiation for three reasons. First, Rojas-Ochoa et al.¹⁹ demonstrated theoretically that the depolarization ratio depends on bulk optical parameters. Since the five types of skin lesions show noticeable differences in their morphology, these distinctions should be reflected in their bulk optical properties, and hence the properties of their polarization speckle. Second, the polarization speckle pattern $D(x, y)$ could be acquired within milliseconds by two CCD cameras simultaneously. The rapid acquisition time resolves the body movement issue which is critical for *in vivo* examination in a clinical setting. Our technique can potentially be developed into a real-time noninvasive application. Finally, the polarization speckle pattern $D(x, y)$ which represents the fraction of light that maintains its initial linear

polarization, was associated with the signal from the more superficial layers where significant skin lesions often originate.

It is known that the first four orders of central moments (central moments are statistical moments after the data distribution is normalized to zero mean) represent mean, variance, skewness and kurtosis of a data distribution.²⁰ In this paper, however, we used statistical moments, which do not hold any extra physical meaning as central moments per se except the first order moment. Nevertheless, central moments and statistical moments are related and statistical moments are used in our paper to represent and quantify the shapes of data distributions. Angelsky et al.¹⁴ demonstrated the analysis of the ellipticities and azimuths of heart, kidney and spleen samples using statistical moments.

Figure 3 illustrates several interesting points. The first order moments M (mean) of the MMs and nevi were generally higher, i.e., having a higher fraction of linear polarized signals, than other lesions for both the blue and red lasers. This phenomenon could be explained by less scattering within MM and nevus due to higher absorption of light by melanin pigment which is present within these types of lesions. In fact, the median values of MM and nevus were either substantially higher or lower than other three types of lesions in all four moments. This difference appeared to be more pronounced for blue versus red illumination light. A possible explanation for the larger differences in the blue data is that there is a bigger difference in the absorption coefficients between pigmented and nonpigmented lesions for the blue versus the red wavelengths.²¹

It is interesting to note that the blue laser showed excellent separation for MM against SK, BCC and SCC, while the red laser was the most effective in separating SK against MM, nevus and BCC. The blue laser results may be explained by the absorption difference among the skin lesion types. However, such an explanation cannot be applied to the red laser because all lesions have somewhat similar absorption coefficients in the red spectral region.²¹ The proper explanation may be associated with the discrepancy in scattering coefficients and/or anisotropy factors. Further investigations and a better understanding of the specific bulk optical properties for different types of skin lesions are required.

Tables 2 and 3 reveal that our technique is most effective for differentiating MM and SK, especially in the higher order of moments, such as the fourth order. Because SK often resembles MM, many optical systems have attempted to develop diagnostic-aided methods to discriminate these two types of lesions. Thus, we could compare the sensitivity and specificity of the fourth order statistical moment of the polarization speckle patterns with the values reported by other researchers. Using the fourth order moment E as a diagnostic discriminator, we generated a receiver operating characteristic (ROC) curve for differentiating MM and SK by plotting the true positive rate (sensitivity) of the indicator against the false positive rate ($1 - \text{specificity}$). The ROC curves of the fourth order statistical moment of polarization speckle pattern for the red and blue lasers are depicted in Fig. 4(a) and 4(b), respectively. Within these figures, we also plotted the sensitivity and specificity values for other studies of MM and SK, such as Raman spectroscopy (open square),²² SIAscope (open triangle),²³ multispectral imaging (open diamond),²⁴ and SolarScan (open circle).²⁵ Note that Lui et al.'s Raman study²² reports three sensitivity and specificity pairs, and they are all included in Fig. 4. In addition, the sensitivity and specificity values for dermatologists specializing

Table 1 Skin lesion types evaluated by speckle imaging.

Skin lesion type	Number of lesions
Malignant melanoma (MM)	25
Squamous cell carcinoma (SCC)	11
Basal cell carcinoma (BCC)	31
Melanocytic nevus (Nevus)	76
Seborrheic keratosis (SK)	71
Total	214

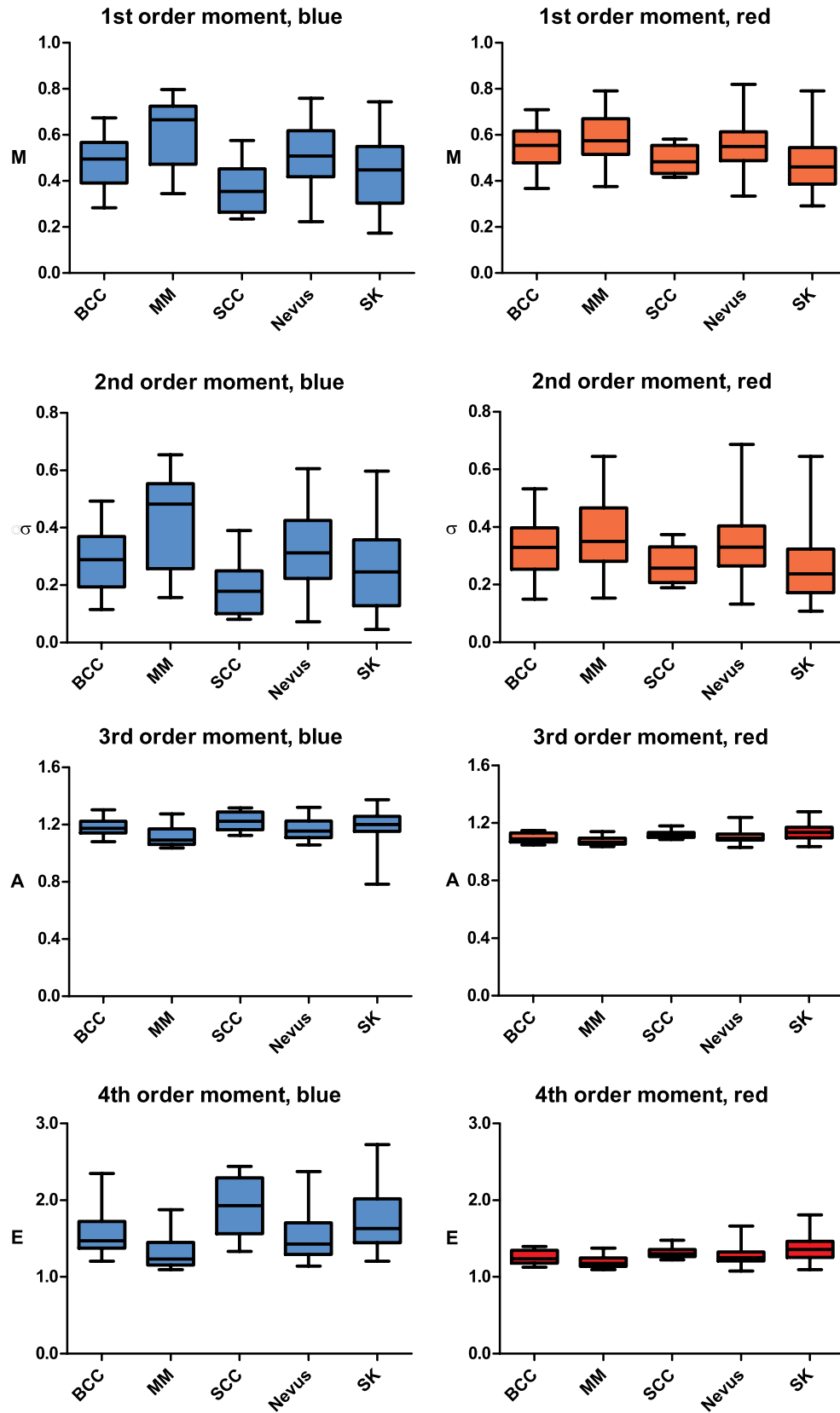


Fig. 3 Four statistical moment distributions for lesion type for the blue (left column) and red (right column) lasers. The bottom and top lines of the box are the 25th and 75th percentile of the data values, respectively, and the central line inside the box indicates the median value. The ends of the whiskers represent the minimum and maximum of the data points.

Table 2 Dunn's multiple comparison tests for the blue laser.

First order moment (M)		Second order moment (σ)		Third order moment (A)		Fourth order moment (E)	
MM versus SK	***	MM versus SK	***	MM versus SK	***	MM versus SK	***
MM versus SCC	***	MM versus SCC	***	MM versus SCC	**	MM versus SCC	***
				MM versus BCC	*	MM versus BCC	*
						Nevus versus SK	*
						Nevus versus SCC	*

Note: The number of asterisks denotes the p values <0.05 (*), <0.01 (**) or <0.001 (***)

Table 3 Dunn's multiple comparison test for the red laser.

First order moment (M)		Second order moment (σ)		Third order moment (A)		Fourth order moment (E)	
SK versus MM	***	SK versus MM	**	SK versus MM	***	SK versus MM	***
SK versus Nevus	***	SK versus Nevus	***	SK versus Nevus	***	SK versus Nevus	***
SK versus BCC	*			SK versus BCC	**	SK versus BCC	**
				SCC versus MM	*	SCC versus MM	*

Note: The number of asterisks denotes the p values <0.05 (*), <0.01 (**) or <0.001 (***)

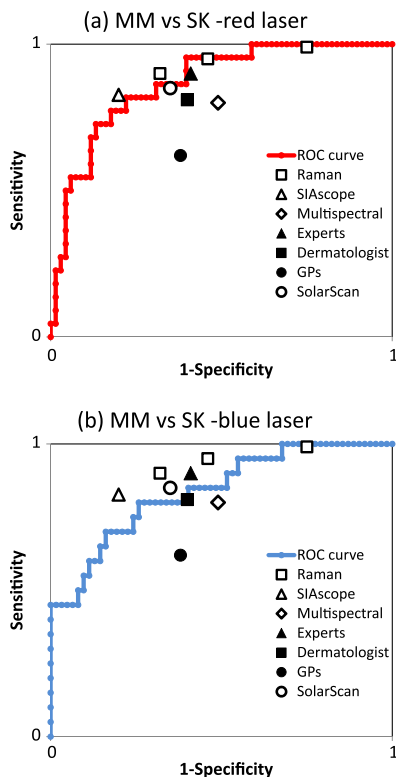


Fig. 4 ROC curves of the fourth order moment E of the polarization speckle patterns for MM and SK using (a) red and (b) blue lasers. Published sensitivity and specificity values for Raman (open square), SIAscope (open triangle), multispectral imaging (open diamond), SolarScan (open circle), dermatologists specialized in melanoma (closed triangle), general dermatologists (closed square), and general practitioners (closed circle) are also included in the plots.

in melanoma, general dermatologists, and general practitioners are also plotted.²⁵ Figure 4(a) shows that our diagnostic indicator using the red laser outperformed the Raman sensitivity/specificity pair with the highest sensitivity (the top open square),²² SolarScan (open circle),²⁵ multispectral imaging (open diamond),²⁴ and all three groups of physicians.²⁵ One of the sensitivity/specificity points of the Raman study (the middle open square)²² is on the ROC curve, indicating this data point has a similar accuracy as our discriminator. Only the Raman result with the lower sensitivity (the lower open square)²² and the SIA-scopy (open triangle)²³ have a slightly better performance than our technique. The area under curve values for the red and blue lasers are 0.87 and 0.84, respectively, indicating that the blue laser results [Fig. 4(b)] are slightly inferior to the red laser results. This fact is also reflected in the comparison of the blue laser results with other studies, in that our discriminator performed similar or better only for one Raman data point (the open square with the highest sensitivity value),²² multispectral imaging (open diamond),²⁴ general dermatologists (close square),²⁵ and general practitioners (close circle).²⁵

5 Conclusions

We demonstrated that the polarization speckle pattern $D(x, y)$, computed from two cross-polarized intensity speckle patterns, has a potential for skin lesion differentiation. In an *in vivo* clinical study involving 214 skin cancers and benign skin lesions, we discovered that the statistical moments of the polarization speckle pattern could separate MM from SK, SCC, and BCC using the blue laser, and separate SK from MM, nevus, and BCC using the red laser. Interestingly, our approach is most effective at differentiating MM and SK, which can often resemble each other clinically leading to a diagnostic dilemma, using a high order moment such as the fourth order moment.

The proposed method is fast and relatively easy to implement. The measurements could be completed within a few milliseconds so that the critical body movement issue for *in vivo* study can be resolved. Our approach could potentially become a real-time application. ROC analysis suggested that our method has a high accuracy similar to many other well-known and accepted diagnostic procedures.

Despite the listed advantages of using polarization speckle for skin cancer diagnosis, the physical process underlying the phenomena are not yet fully understood and require further study. We believe that this experimental study will inspire further development of the polarization speckle technique.

Acknowledgments

This work was supported in part by grants from the Canadian Dermatology Foundation, Canadian Institutes of Health Research, Natural Sciences and Engineering Research Council of Canada, UBC & VGH Hospital Foundation, and UBC Faculty of Medicine.

References

1. N. Ghosh and I. A. Vitkin, "Tissue polarimetry: concepts, challenges, applications, and outlook," *J. Biomed. Opt.* **16**(11), 110801 (2011).
2. American Cancer Society, *Cancer facts and figures 2011*, American Cancer Society, Atlanta (2012).
3. Canadian Cancer Society's Steering Committee, *Canadian Cancer Statistics 2012*, Canadian Cancer Society, Toronto, Ontario (2012).
4. C. M. Balch et al., "Final version of 2009 AJCC melanoma staging and classification," *J. Clin. Oncol.* **27**(36), 6199–6206 (2009).
5. Y. Pan et al., "Polarized and nonpolarized dermoscopy: the explanation for the observed differences," *Arch. Dermatol.* **144**(6), 828–829 (2008).
6. Y. Liu et al., "Investigation of depth selectivity of polarization gating for tissue characterization," *Opt. Express* **13**(2), 601–611 (2005).
7. G. Argenziano et al., "Dermoscopy of pigmented skin lesions: Results of a consensus meeting via the Internet," *J. Am. Acad. Dermatol.* **48**(5), 679–693 (2003).
8. S. L. Jacques, J. C. Ramella-Roman, and K. Lee, "Imaging skin pathology with polarized light," *J. Biomed. Opt.* **7**(3), 329–340 (2002).
9. S. P. Morgan and I. Stockford, "Surface-reflection elimination in polarization imaging of superficial tissue," *Opt. Lett.* **28**(2), 114–116 (2003).
10. E. Salomatina et al., "Optical properties of normal and cancerous human skin in the visible and near-infrared spectral range," *J. Biomed. Opt.* **11**(6), 064026 (2006).
11. J. C. Maize and A. B. Ackerman, *Pigmented Lesions of the Skin*, Lea & Febiger, Philadelphia (1987).
12. M. F. Wood et al., "Proof-of-principle demonstration of a Mueller matrix decomposition method for polarized light tissue characterization *in vivo*," *J. Biomed. Opt.* **14**(1), 014029 (2009).
13. O. V. Angelsky et al., "Polarization singularities of the object field of skin surface," *J. Phys. D: Appl. Phys.* **39**(16), 3547–3558 (2006).
14. O. V. Angelsky et al., "Polarization-correlation mapping of biological tissue coherent images," *J. Biomed. Opt.* **10**(6), 064025 (2005).
15. F. Boulvert et al., "Analysis of the depolarizing properties of irradiated pig skin," *J. Opt. A: Pure Appl. Opt.* **7**(1), 21–28 (2005).
16. J. W. Goodman, *Speckle Phenomena in Optics: Theory and Application*, Roberts and Company Publishers, Greenwood Village, CO (2006).
17. D. J. Gawkrödger, *Dermatology: An Illustrated Colour Text*, 2nd ed., Churchill Livingstone, New York (1997).
18. K. Phillips et al., "Time-resolved ring structure of circularly polarized beams backscattered from forward scattering media," *Opt. Express* **13**(20), 7954–7969 (2005).
19. L. F. Rojas-Ochoa et al., "Depolarization of backscattered linearly polarized light," *J. Opt. Soc. Am. A* **21**(9), 1799–1804 (2004).
20. W. H. Press, *Numerical Recipes in C: The Art of Scientific Computing*, 2nd ed., Cambridge University Press, Cambridge, New York (1992).
21. A. Garcia-Urbe et al., "In vivo diagnosis of melanoma and nonmelanoma skin cancer using oblique incidence diffuse reflectance spectrometry," *Cancer Res.* **72**(11), 2738–2745 (2012).
22. H. Lui et al., "Real-time Raman spectroscopy for in vivo skin cancer diagnosis," *Cancer Res.* **72**(10), 2491–2500 (2012).
23. M. Moncrieff et al., "Spectrophotometric intracutaneous analysis: A new technique for imaging pigmented skin lesions," *Brit. J. Dermatol.* **146**(3), 448–457 (2002).
24. B. Farina et al., "Multispectral imaging approach in the diagnosis of cutaneous melanoma: Potentiality and limits," *Phys. Med. Biol.* **45**(5), 1243–1254 (2000).
25. S. W. Menzies et al., "The performance of SolarScan: an automated dermoscopy image analysis instrument for the diagnosis of primary melanoma," *Arch. Dermatol.* **141**(11), 1388–1396 (2005).